Imaging Findings of Mass-Forming Intrahepatic Cholangiocarcinoma

Subjects: Oncology

Contributor: Aleksandra Djikic Rom, Jelena Kovac, Aleksandra Jankovic, Nikica Grubor

Intrahepatic cholangiocarcinoma (ICC) is the second most common primary hepatic malignancy, with mass-forming growth pattern being the most common. The typical imaging appearance of mass-forming ICC (mICC) consists of irregular ring enhancement in the arterial phase followed by the progressive central enhancement on portal venous and delayed phases. However, atypical imaging presentation in the form of hypervascular mICC might also be seen, which can be attributed to distinct pathological characteristics. Ancillary imaging features such as lobular shape, capsular retraction, segmental biliary dilatation, and vascular encasement favor the diagnosis of mICC.

Keywords: mass-forming cholangiocarcinoma ; mimickers ; magnetic resonance imaging

1. Introduction

Intrahepatic cholangiocarcinoma (ICC) is the second most common primary malignant liver tumor after hepatocellular carcinoma (HCC) [1]. These tumors arise from the intrahepatic biliary duct epithelium, proximal to the second-order bile ducts [2]. Although the majority of cases occur sporadically, there are certain medical conditions that are considered to be risk factors for ICC development, in particular primary sclerosing cholangitis (PSC), choledochal cyst, intrahepatic lithiasis, Caroli disease, clonorchiasis, and viral hepatitis (especially type C) [3][4].

According to the growth pattern, ICC can be classified into mass-forming, periductal-infiltrating, or intraductal growth types [5]. Among the three different growth patterns, mass-forming cholangiocarcinoma (mICC) is the most common, accounting for 80% of all cases [5]. The second most common type is mixed type consisting of mass-forming and periductal infiltrating growth pattern [5]. Even though mixed type was initially introduced as a distinctive type, it is now grouped together with mass-forming type according to its imaging presentation [5][6]. However, recent studies have shown that gross morphological classification is insufficient in explaining the atypical presentations of ICC [7]. In order to provide better understanding of varying imaging appearances of mICC and its correlation with clinicopathological features, Kim et al. have proposed new dichotomous imaging classification introducing “parenchymal” and “ductal” types of mICC [8]. This is in accordance with the new histological classification that divides ICC into small duct and large duct types [9]. With regard to new imaging classification, parenchymal type originates from small bile ducts or canals of Hering and presents as a mass-forming lesion without gross involvement or bile duct dilatation [8]. On the other hand, ductal type develops from mature cholangiocytes of the large bile ducts and presents usually as mixed mass-forming and periductal infiltrating lesion causing biliary dilatation [8][10]. In addition, it has been shown that the ductal type tends to show hypovascularity while the parenchymal type frequently displays hypervascularity on imaging studies [11][12]. Furthermore, Hayashi et al. have shown that large bile duct type was more commonly associated with poor differentiation due to the rich fibrous stroma in contrast to the small duct type, which had better postsurgical outcomes [12][13]. Therefore, recognition of this different imaging appearances of mICC provides additional clinical information regarding the prognosis and clinical outcome, which may influence treatment decisions in certain cases [8].

2. Imaging Findings of Mass-Forming ICC

The imaging appearance of mICC depends on its pathohistological composition and is determined by the amount of fibrous stroma, viable tumor cells, intralesional mucin, and necrosis [14].

2.1. Typical Imaging Features of mICC

Mass-forming ICC typically presents as a large, lobulated, irregularly shaped lesion with well-defined borders [14]. On MRI, the tumor is usually hypointense on T1-weighted images, while the appearance on T2-weighted images varies from hypointensity in highly fibrotic lesions to hyperintensity in necrotic or mucin-rich tumors [15]. Although central T2-weighted

hypointensity is considered a characteristic MRI feature of mICC, it can also be seen in colorectal metastasis due to intralesional coagulative necrosis [14]. Nevertheless, in most of the cases mICC presents as a heterogeneous lesion on T2-weighted images containing both areas of hyperintensity and areas of hypointensity [14][15]. The characteristic enhancement pattern using conventional gadolinium-based extracellular agents consists of an irregular ring enhancement on the arterial phase followed by progressive central enhancement in the portal venous and delayed phases (**Figure 1**) [14][15]. This postcontrast behavior could be explained by a rim of viable cells at the periphery of the tumor and rich edematous internal fibrous stroma [15].

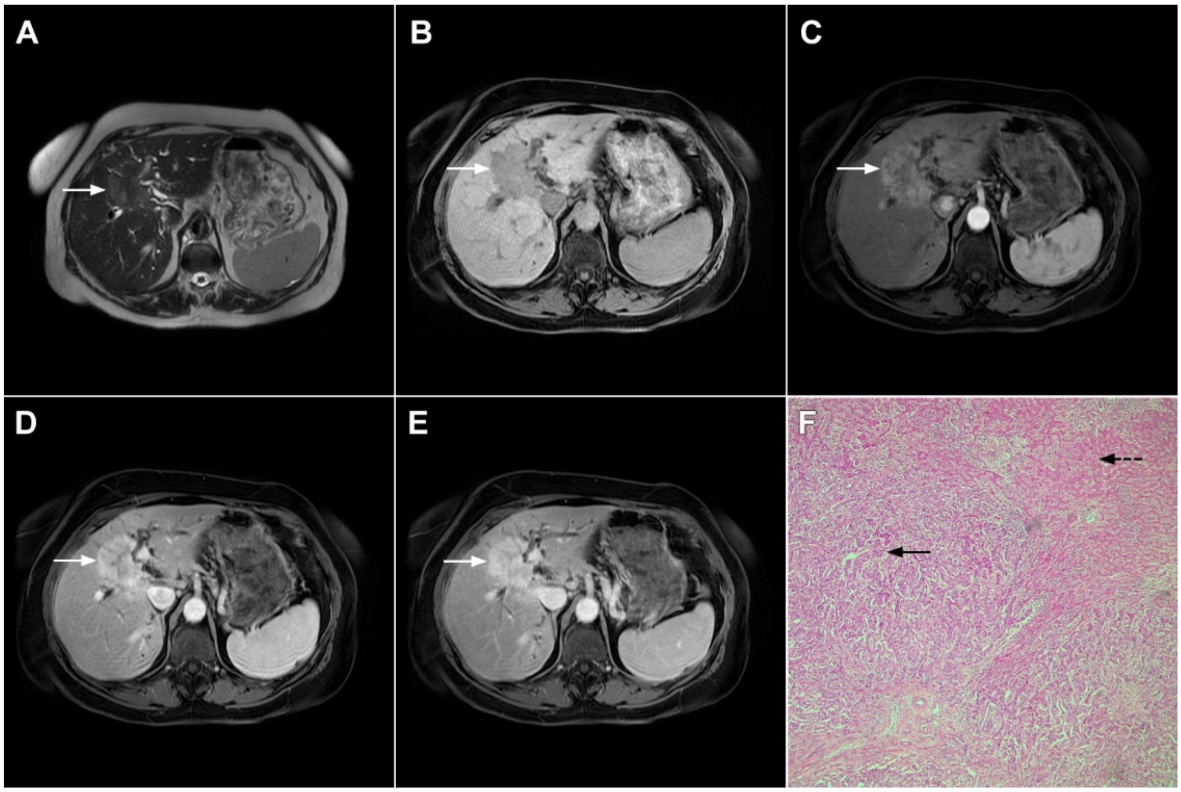

Figure 1. Typical intrahepatic mass-forming cholangiocarcinoma in 68-year-old woman. On axial T2-weighted image a lobular heterogeneously hyperintense tumor (*arrow*) is seen, located centrally in the liver segment IVB (**A**). The lesion (*arrow*) is hypointense in a plain T1-weighted image (**B**) with irregular ring enhancements in the arterial phase (**C**) and progressive enhancement in the portalvenous (**D**) and delayed phase (**E**). Note the perilesional biliary dilatation. Hematoxylin and eosin (H&E) staining (**F**) showed cholangiocarcinoma (*arrow*) and normal liver parenchyma next to the tumor (*dashed arrow*); original magnification ×40.

However, in highly fibrotic lesions or in lesions with internal necrosis, central parts may remain non-opacified even on delayed images (**Figure 2**) [14].

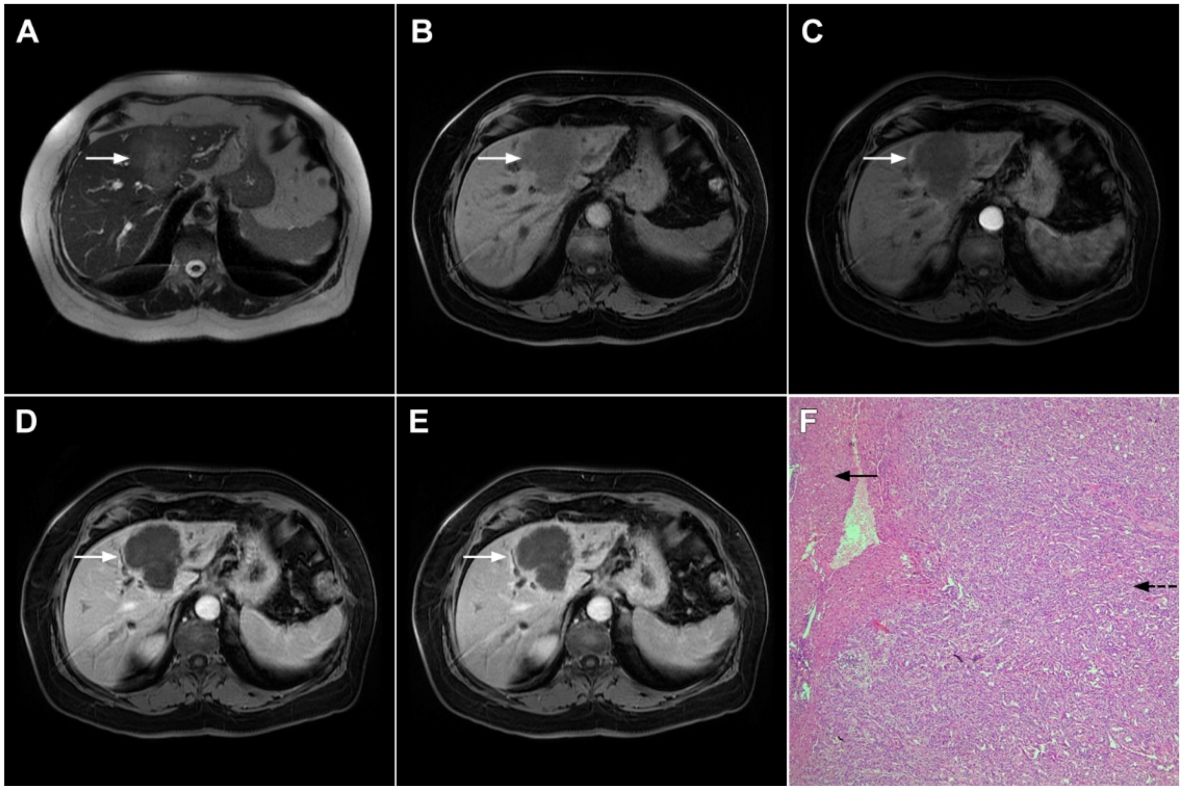

Figure 2. Mass-forming intrahepatic cholangiocarcinoma in 72-year-old man. Irregular heterogeneously hyperintense lesion (*arrow*) on T2-weighted image (**A**) located in liver segments IVB and III with peripheral biliary dilatation is shown. On a plain T1-weighted image (**B**) the lesion (*arrow*) is hypointense with only discrete ring enhancement in the arterial phase (**C**) but without detectable enhancements in the portal venous (**D**) and delayed phases (**E**). Hematoxylin and eosin (H&E) staining (**F**) showed poorly differentiated cholangiocarcinoma (*dashed arrow*); normal liver parenchyma is also shown (*arrow*); original magnification ×40.

Target sign, consisting of diffusion restriction at the periphery of the lesion and low signal intensity in its central parts on high-*b*-value diffusion weighted imaging (DWI), could be considered to be a pathognomonic finding in mICC [16][17]. It can be attributed to the loose central fibrotic stroma with accompanying edema that is responsible for low signal intensity in DWI, while the periphery of the lesion is composed of densely packed viable tumor cells that cause diffusion restriction and dark rings on the apparent diffusion coefficient (ADC) map (**Figure 3**) [16].

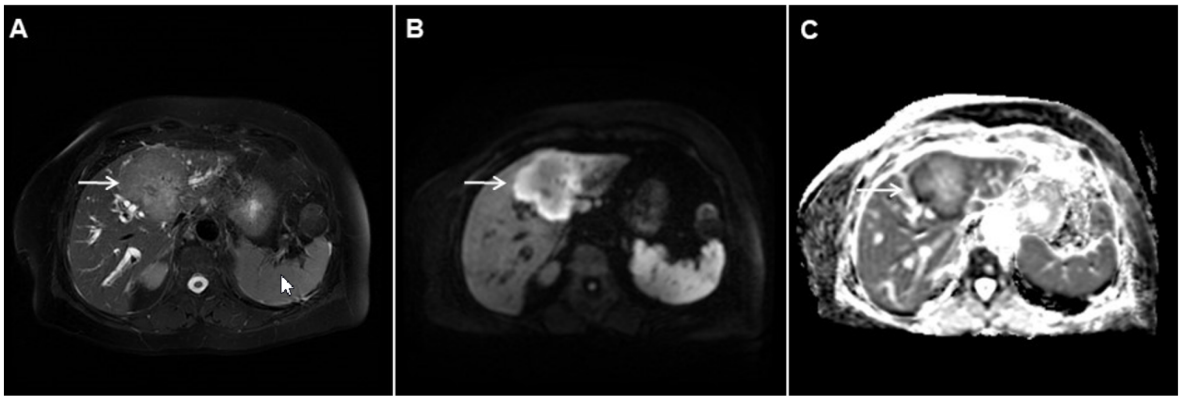

Figure 3. Mass-forming intrahepatic cholangiocarcinoma in the left liver lobe of a 76-year-old man. Axial T2-weighted FS image shows lobulated hetrogeneously hyperintense hepatic tumor (*arrow*) with perilesional biliary dilatation (**A**). Axial diffusion-weighted image (b = 800 s/mm^2) shows target-like appearance (*arrow*) of the lesion that consists of a central darker area and a peripheral hyperintense area (**B**). Corresponding ADC map is shown on (**C**).

If hepatocyte-selective contrast media are used, mICC presents typically as hypointense lesions on the hepatobiliary phase due to the lack of functional hepatocytes with a sharp margin between the tumor and the background liver parenchyma [7]. Thus, tumor size as well as the presence of perilesional satellite nodules, could be more precisely evaluated in the hepatobiliary phase in comparison to the MRI with conventional extracellular contrast [18][19]. Additionally, the “cloud sign”, seen as a relatively high cloud-like signal intensity in the central part of the lesion surrounded by a hypointense peripheral rim, is considered characteristic of mICC (**Figure 4**) [19]. The appearance of mICC in the

hepatobiliary phase may be used as a prognostic factor since it correlates well with the content of intralesional fibrous stroma [20]. Namely, if cloud sign is seen it indicates a large amount of fibrous stroma in the central parts of the tumor, which is frequently associated with poor prognosis [20]. Additional imaging features, which are shown to be prognostic factors and can be assessed in the hepatobiliary phase, include capsule penetration and hepatic vein obstruction, as was demonstrated in the study by Kim S et al. [21].

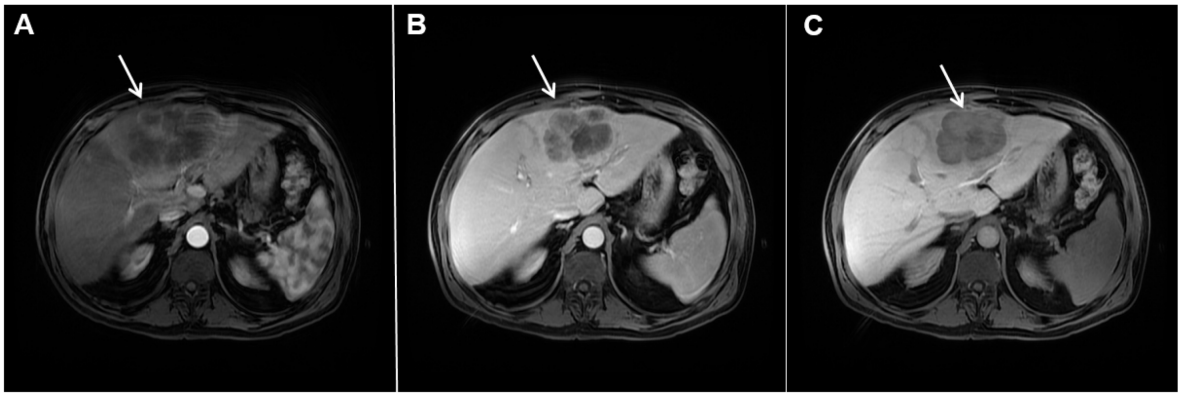

Figure 4. Mass-forming intrahepatic cholangiocarcinoma in a 68-year-old woman. Axial T1-weighted image after gadoxetic acid administration obtained in arterial phase (**A**) shows peripherally enhancing lesion (*arrow*). Portal venous phase in the same patient (**B**) shows progressive centripetal enhancement of the lesion (*arrow*) with cloud-like appearance in the hepatobiliary phase (**C**) consisting of an area of central enhancement and a thin, peripheral, hypointense rim.

Ancillary MRI findings that are frequently seen in mICC include peripheral biliary dilatation, capsular retraction, vascular encasement, lobar atrophy, satellite nodules, and lymphadenopathy [15][16]. Nevertheless, it should be kept in mind that in the parenchymal type of mICC, due to its origin from the small bile ducts, ancillary features such as biliary dilatation, vascular encasement, and lobar atrophy may be absent (**Figure 5**). In such cases, the presence of typical postcontrast behavior and capsular retraction indicate mICC. On the other hand, some degree of obstruction and peripheral bile duct dilatation is always seen in the ductal type of mICC [15].

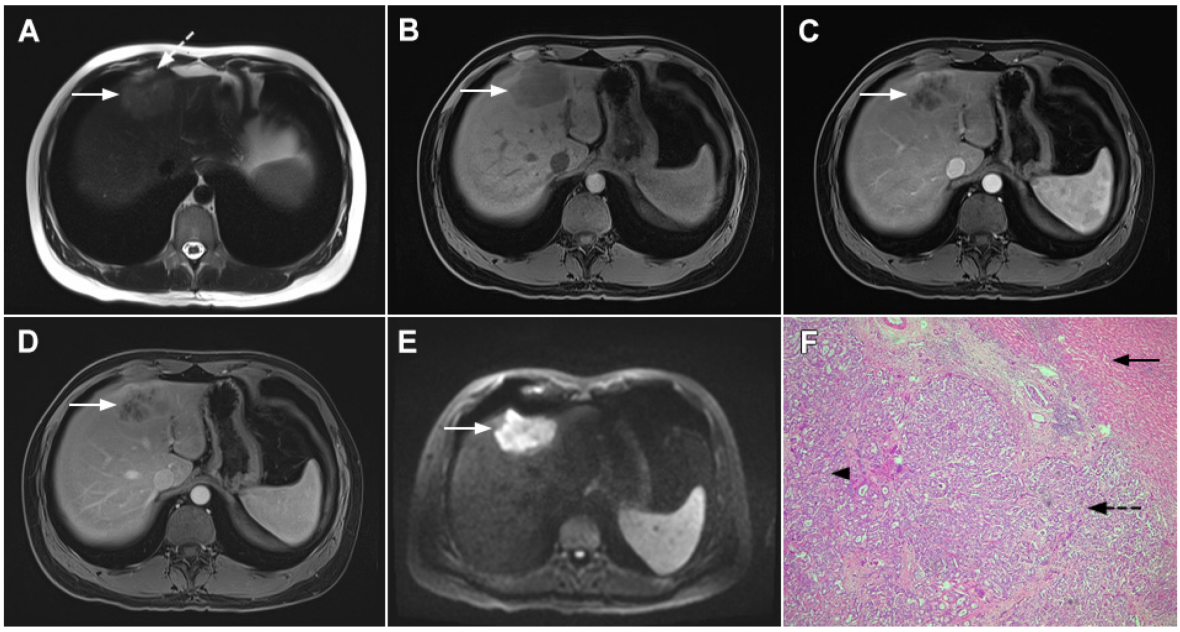

Figure 5. Parenchymal mass-forming cholangiocarcinoma in a 36-year-old man. The lobular slightly hyperintense lesion (*arrow*) is seen in the liver segment IVA in a T2-weighted image (**A**) with subtle capsular retraction (*dashed arrow*). On a plain T1-weighted image (**B**), the tumor (*arrow*) is hypointense with irregular discrete peripheral and central enhancements in the arterial phase (**C**), mild progressive enhancement in the portal venous phase (**D**), and high signal intensity in DWI (**E**). Hematoxylin and eosin (H&E) staining (**F**) showed cholangiocarcinoma (*arrowhead*) with poorly differentiated components (*dashed arrow*). Normal liver parenchyma is also shown (*arrow*); original magnification ×40.

Although capsular retraction is considered to be a characteristic finding for mICC [14][15], it can also be observed in many other lesions with abundant fibrosis and desmoplasia, such as metastatic colon carcinoma, scirrhous hepatocellular carcinoma, and hemangioendothelioma [22]. Therefore, this sign must be evaluated only in combination with other imaging

findings. Due to its infiltrative growth, mICC may lead to vascular encasement, resulting in lobar or segmental parenchymal atrophy [14][15]. In contrast to HCC, mICC rarely leads to tumor thrombus formation [23]. Satellite lesions around the main tumor are frequent findings probably due to the invasion of adjacent small portal vein branches [19]. The formation of satellite nodules, and their subsequent fusion with the main tumor, results in the lobular shape of the lesion, which is shown to be a characteristic feature of mICC [19]. Lymphadenopathy in porta hepatis, and hepatoduodenal ligament can be seen in up to 73% of mICC cases but is a nonspecific finding [15].

2.2. Atypical Imaging Features of mICC

Besides the typical imaging presentation of mICC, atypical appearance can also be observed in imaging studies [24]. Hypervascular mICCs are usually small lesions and this vascular behavior might be explained by less intralesional fibrosis and abundant vascular stroma [25]. The incidence of hypervascular mICC ranges from 12.5% up to 47% in previous reports [18][25]. Since hypervascular mICCs are frequently seen in cirrhotic livers, the differential diagnosis with HCC may be very difficult. In this regard, the absence of washout and the presence of progressive enhancement together with the lack of fibrous pseudocapsule favor the diagnosis of mICC over HCC [25]. However, if hypervascular mICC shows washout in the portal venous phase, preoperative differential diagnosis with HCC is hardly possible (**Figure 6**). In such cases, additional findings, such as cloud appearance in the hepatobiliary phase, multiplicity around the main tumor, or intrahepatic metastasis, capsule retraction and tumor markers may be helpful for differentiating between these tumors [18][19]. Hypervascular mICC differs from typical hypovascular mICC not only in terms of vascularity but also in patient outcome, as it has been shown that the former has much better prognosis [12]. Therefore, the assessment of tumor vascularity on preoperative imaging could represent an important marker for predicting malignant characteristics in mICC [26].

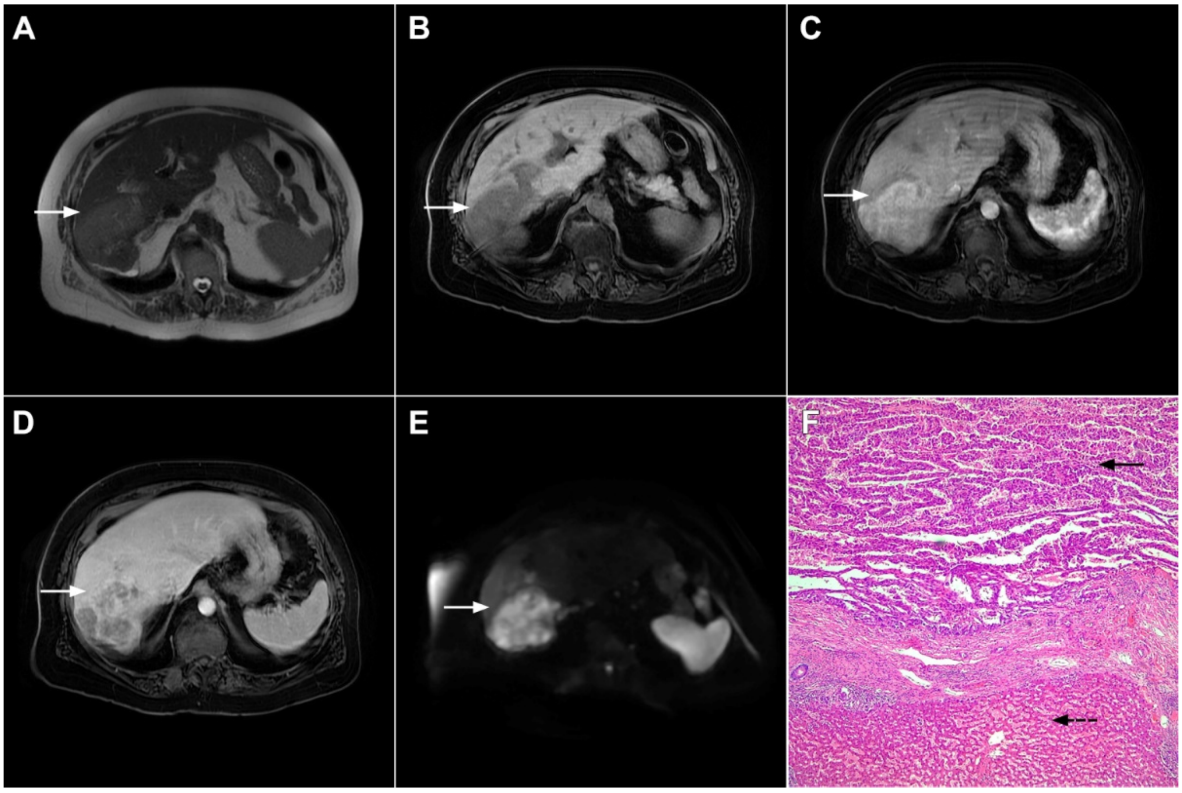

Figure 6. Hypervascular mass-forming cholangiocarcinoma in a 63-year-old woman. The axial T2-weighted image (**A**) shows a moderately hyperintense tumor (*arrow*) located in liver segments VI and VII with a subtle medial capsular retraction. The lesion (*arrow*) is hypointense on the plain T1-weighted image (**B**), hypervascular in the arterial phase (**C**) with washout on the portal venous phase (**D**). The tumor (*arrow*) is hyperintense on DWI (**E**). Hematoxylin and eosin (H&E) staining (**F**) showed well-differentiated cholangiocarcinoma (*arrow*) surrounded by normal liver parenchyma (*dashed arrow*); original magnification ×40.

Mucinous cholangiocarcinoma is a rare variant of mICC characterized by rich mucin production [24][27]. According to previous studies, mucinous mICC originate from mucin-producing cholangiocytes located in large bile ducts [28]. Imaging findings in mucinous mICC reflect characteristic histopathological features of the lesion with cancer cell nests suspended in a large mucinous lake [29]. Therefore, these lesions display strong T2-weighted hyperintensity [27]. Moreover, as cancer cells in the center of the lesion are scarce, these tumors show only slight progressive enhancement of intralesional septa and cellular nests in postcontrast studies (**Figure 7**) [27]. Due to its very high signal intensity on T2-weighted images and

centripetal pattern of enhancement, mucinous mICC may be misdiagnosed as hemangiomas [29]. Concerning similarities in the postcontrast behavior of mucinous mICC and hemangiomas, it should be kept in mind that mICC displays continuous ragged rim enhancements in contrast to the discontinuous, stronger peripheral and centripetal enhancement following the blood pool seen in hemangiomas [24][29].

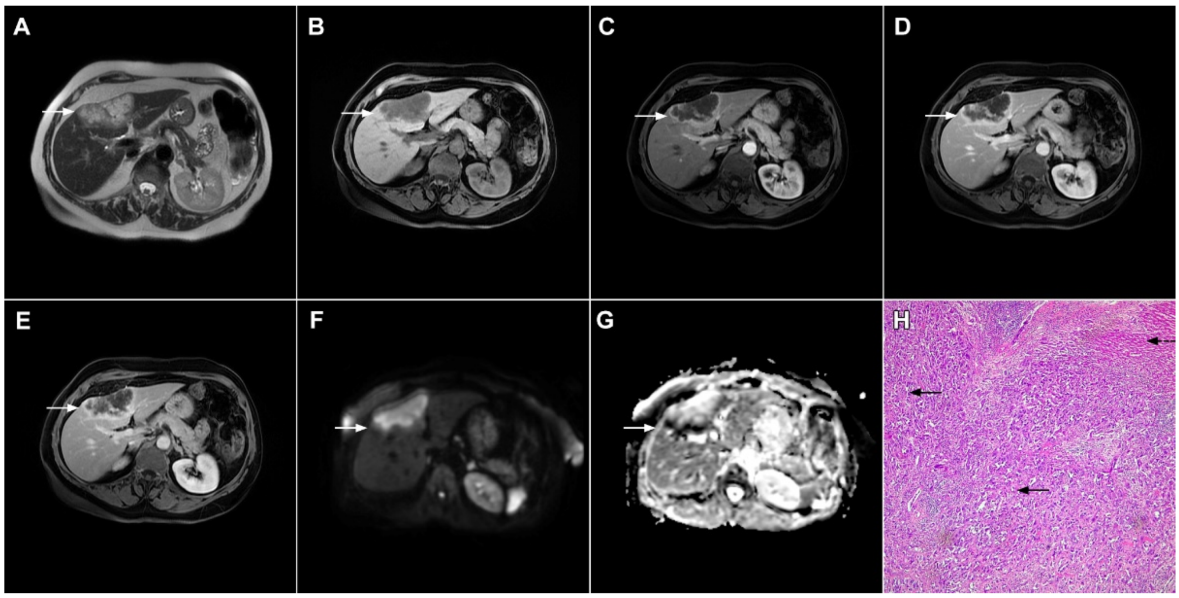

Figure 7. Mucin-rich mass-forming cholangiocarcinoma in a 78-year-old woman. The axial T2-weighted image (**A**) shows the lobulated hyperintense lesion (*arrow*) located in the subcapsular region of liver segment IVB, which is associated with capsular retraction. On the plain T1-weighted image (**B**) the lesion (*arrow*) is hypointense. In the arterial phase (**C**), ring enhancement can be seen with slight “ragged” central enhancement in the portal venous (**D**) and delayed phase (**E**). On DWI, diffusion restriction is noted on the periphery of the lesion (*arrow*) while no restriction is seen in the central part of the tumor (**F**). Corresponding ADC map showing targetoid appearance of the lesion is shown on (**G**). Hematoxylin and eosin (H&E) staining (**H**) showed cholangiocarcinoma (*arrows*) adjacent to normal liver parenchyma (*dashed arrow*); original magnification ×40.

References

1. Choi, B.I.; Lee, J.M.; Han, J.K. Imaging of intrahepatic and hilar cholangiocarcinoma. Abdom. Imaging 2004, 29, 548–557.
2. Lazaridis, K.N.; Gores, G.J. Cholangiocarcinoma. Gastroenterology 2005, 128, 1655–1667.
3. Shaib, Y.H.; El-Serag, H.B.; Nooka, A.K.; Thomas, M.; Brown, T.D.; Patt, Y.Z.; Hassan, M.M. Risk factors for intrahepatic and extrahepatic cholangiocarcinoma: A hospital-based case-control study. Am. J. Gastroenterol. 2007, 102, 1016–1021.
4. El-Diwany, R.; Pawlik, T.M.; Ejaz, A. Intrahepatic Cholangiocarcinoma. Surg. Oncol. Clin. N. Am. 2019, 28, 587–599.
5. Lim, J.H. Cholangiocarcinoma: Morphologic classification according to growth pattern and imaging findings. AJR Am. J. Roentgenol. 2003, 181, 819–827.
6. Yamasaki, S. Intrahepatic cholangiocarcinoma: Macroscopic type and stage classification. J. Hepatobiliary Pancreat. Surg. 2003, 10, 288–291.
7. Jeong, H.T.; Kim, M.J.; Chung, Y.E.; Choi, J.Y.; Park, Y.N.; Kim, K.W. Gadoxetate disodium-enhanced MRI of mass-forming intrahepatic cholangiocarcinomas: Imaging-histologic correlation. AJR Am. J. Roentgenol. 2013, 201, W603–W611.
8. Kim, M.J.; Rhee, H.; Woo, H.Y. A dichotomous imaging classification for cholangiocarcinomas based on new histologic concepts. Eur. J. Radiol. 2019, 113, 182–187.
9. Nakanuma, Y.; Sato, Y.; Harada, K.; Sasaki, M.; Xu, J.; Ikeda, H. Pathological classification of intrahepatic cholangiocarcinoma based on a new concept. World J. Hepatol. 2010, 2, 419–427.
10. Cardinale, V.; Carpino, G.; Reid, L.; Gaudio, E.; Alvaro, D. Multiple cells of origin in cholangiocarcinoma underlie biological, epidemiological and clinical heterogeneity. World J. Gastrointest. Oncol. 2012, 4, 94–102.

11. Fujita, N.; Asayama, Y.; Nishie, A.; Ishigami, K.; Ushijima, Y.; Takayama, Y.; Okamoto, D.; Moirta, K.; Shirabe, K.; Aishima, S.; et al. Mass-forming intrahepatic cholangiocarcinoma: Enhancement patterns in the arterial phase of dynamic hepatic CT-Correlation with clinicopathological findings. Eur. Radiol. 2017, 27, 498–506.
12. Nam, J.G.; Lee, J.M.; Joo, I.; Ahn, S.J.; Park, J.Y.; Lee, K.B.; Han, J.K. Intrahepatic Mass-Forming Cholangiocarcinoma: Relationship Between Computed Tomography Characteristics and Histological Subtypes. J. Comput. Assist. Tomogr. 2018, 42, 340–349.
13. Hayashi, A.; Misumi, K.; Shibahara, J.; Arita, J.; Sakamoto, Y.; Hasegawa, K.; Kokudo, N.; Fukayama, M. Distinct Clinicopathologic and Genetic Features of 2 Histologic Subtypes of Intrahepatic Cholangiocarcinoma. Am. J. Surg. Pathol. 2016, 40, 1021–1030.
14. Jhaveri, K.S.; Hosseini-Nik, H. MRI of cholangiocarcinoma. J. Magn. Reson. Imaging 2015, 42, 1165–1179.
15. Maetani, Y.; Itoh, K.; Watanabe, C.; Shibata, T.; Ametani, F.; Yamabe, H.; Konishi, J. MR imaging of intrahepatic cholangiocarcinoma with pathologic correlation. AJR Am. J. Roentgenol. 2001, 176, 1499–1507.
16. Park, H.J.; Kim, Y.K.; Park, M.J.; Lee, W.J. Small intrahepatic mass-forming cholangiocarcinoma: Target sign on diffusion-weighted imaging for differentiation from hepatocellular carcinoma. Abdom. Imaging 2013, 38, 793–801.
17. Kovač, J.D.; Galun, D.; Đurić-Stefanović, A.; Lilić, G.; Vasin, D.; Lazić, L.; Mašulović, D.; Šaranović, Đ. Intrahepatic mass-forming cholangiocarcinoma and solitary hypovascular liver metastases: Is the differential diagnosis using diffusion-weighted MRI possible? Acta Radiol. 2017, 58, 1417–1426.
18. Kim, S.H.; Lee, C.H.; Kim, B.H.; Kim, W.B.; Yeom, S.K.; Kim, K.A.; Park, C.M. Typical and atypical imaging findings of intrahepatic cholangiocarcinoma using gadolinium ethoxybenzyl diethylenetriamine pentaacetic acid-enhanced magnetic resonance imaging. J. Comput. Assist. Tomogr. 2012, 36, 704–709.
19. Kang, Y.; Lee, J.M.; Kim, S.H.; Han, J.K.; Choi, B.I. Intrahepatic mass-forming cholangiocarcinoma: Enhancement patterns on gadoxetic acid-enhanced MR images. Radiology 2012, 264, 751–760.
20. Koh, J.; Chung, Y.E.; Nahm, J.H.; Kim, H.Y.; Kim, K.S.; Park, Y.N.; Kim, M.J.; Choi, J.Y. Intrahepatic mass-forming cholangiocarcinoma: Prognostic value of preoperative gadoxetic acid-enhanced MRI. Eur. Radiol. 2016, 26, 407–416.
21. Kim, S.; An, C.; Han, K.; Kim, M.J. Gadoxetic acid enhanced magnetic resonance imaging for prediction of the postoperative prognosis of intrahepatic mass-forming cholangiocarcinoma. Abdom. Radiol. 2019, 44, 110–121.
22. Soyer, P.; Bluemke, D.A.; Vissuzaine, C.; Beers, B.V.; Barge, J.; Levesque, M. CT of hepatic tumors: Prevalence and specificity of retraction of the adjacent liver capsule. AJR Am. J. Roentgenol. 1994, 162, 1119–1122.
23. Han, J.K.; Choi, B.I.; Kim, A.Y.; An, S.K.; Lee, J.W.; Kim, T.K.; Kim, S.W. Cholangiocarcinoma: Pictorial essay of CT and cholangiographic findings. Radiographics 2002, 22, 173–187.
24. Lee, W.J.; Lim, H.K.; Jang, K.M.; Kim, S.H.; Lee, S.J.; Lim, J.H.; Choo, I.W. Radiologic spectrum of cholangiocarcinoma: Emphasis on unusual manifestations and differential diagnoses. Radiographics 2001, 21, S97–S116.
25. Kim, S.A.; Lee, J.M.; Lee, K.B.; Kim, S.H.; Yoon, S.H.; Han, J.K.; Choi, B.I. Intrahepatic mass-forming cholangiocarcinomas: Enhancement patterns at multiphasic CT, with special emphasis on arterial enhancement pattern--correlation with clinicopathologic findings. Radiology 2011, 260, 148–157.
26. Ariizumi, S.; Kotera, Y.; Takahashi, Y.; Katagiri, S.; Chen, I.P.; Ota, T.; Yamamoto, M. Mass-forming intrahepatic cholangiocarcinoma with marked enhancement on arterial-phase computed tomography reflects favorable surgical outcomes. J. Surg. Oncol. 2011, 104, 130–139.
27. Hayashi, M.; Matsui, O.; Ueda, K.; Kadoya, M.; Yoshikawa, J.; Gabata, T.; Takashima, T.; Izumi, R.; Nakanuma, Y. Imaging findings of mucinous type of cholangiocellular carcinoma. J. Comput. Assist. Tomogr. 1996, 20, 386–389.
28. Vijgen, S.; Terris, B.; Rubbia-Brandt, L. Pathology of intrahepatic cholangiocarcinoma. Hepatobiliary Surg. Nutr. 2017, 6, 22–34.
29. Chung, Y.E.; Kim, M.J.; Park, Y.N.; Choi, J.Y.; Pyo, J.Y.; Kim, Y.C.; Cho, H.J.; Kim, K.A.; Choi, S.Y. Varying appearances of cholangiocarcinoma: Radiologic-pathologic correlation. Radiographics 2009, 29, 683–700.